Solar Energy Materials and Solar Cells 201 (2019) 110090

Contents lists available at ScienceDirect

Solar Energy Materials and Solar Cells

journal homepage: www.elsevier.com/locate/solmat

Development of 2D-Mt/SA/AgNPs microencapsulation phase change materials for solar energy storage with enhancement of thermal conductivity and latent heat capacity

Weiquan Zhan[a], Yunliang Zhao[b,c,*], Yuan Yuan[b], Hao Yi[a,**], Shaoxian Song[a]

[a] Hubei Key Laboratory of Mineral Resources Processing and Environment, Wuhan University of Technology, Luoshi Road 122, Wuhan, Hubei, 430070, China
[b] School of Resources and Environmental Engineering, Wuhan University of Technology, Luoshi Road 122, Wuhan, Hubei, 430070, China
[c] Materials Research Institute, The Pennsylvania State University, University Park, PA, 16802, USA

ARTICLE INFO

Keywords:
AgNPs
Two-dimensional montmorillonite
Thermal conductivity
Latent heat capacity
Light-thermal conversion

ABSTRACT

Application of clay mineral based phase change materials (PCMs) on solar energy storage was limited by poor latent heat storage and thermal conductivity. In this study, two-dimensional montmorillonite/stearic acid/Ag nanoparticles (2D-Mt/SA/AgNPs) composites were prepared to enhance the latent heat capacity and thermal transfer ability. It was found that the composites possessed ultra-high latent heat storage (> 187 J/g) and contained more than 90 wt% of SA. Besides, 2D-Mt/SA/AgNPs showed 229.3% increase in thermal conductivity after incorporation of AgNPs into the core of composite PCMs, compared with pure SA. In addition, 2D-Mt/SA/AgNPs exhibited remarkable thermal charging/discharging rate and outstanding light-thermal conversion ability due to the excellent heat transfer ability. Because of the excellent thermal stability and structure reliability, 2D-Mt/SA/AgNPs showed superior cycling performances in the heating/cooling tests. As a consequence, 2D-Mt/SA/AgNPs were promising sustainable energy storage materials owing to large latent heat, high thermal conductivity, outstanding thermal stability and excellent cycling performance.

1. Introduction

In recent years, renewable energy had been widely studied owing to excessive use of fossil energy and serious environmental pollution problems [1–3]. Solar energy, as most environmental and freest energy, had been considered as the best candidate for solving energy crisis [4–6]. Phase change materials (PCMs) could convert solar energy to thermal energy during phase transition, thus it has been widely used as solar energy storage media [7–9]. In fact, PCMs had been extensively researched in application for thermal energy storage recent years, such as building energy [10], air conditional [11] and other sustainable fields [12]. However, the practical application of PCMs was seriously restricted by the limited latent heat capacity and poor thermal conductivity.

It was vital to store massive energy in a much smaller space [13,14]. Nevertheless, supporting materials which were used to prevent leakage often occupied very large volume in the composite PCMs, leading to limited thermal energy storage capacity. Previously, diatomite [15], montmorillonite (Mt) [16], vermiculite [17] *etc.* were employed for storing organic PCM in pore and interlayer space. However, for the limited pore or interlayer space, the composite PCMs had very low latent heat. Then microcapsule structure of composite PCMs was proposed for enhancing latent heat storage [18]. But, the composite PCMs still possessed low latent heat owing to high weight of shell. Recently, two-dimensional materials were applied for encapsulating PCMs to promote energy storage performances because they had ultra-high surface area and very thin thickness [19,20]. Graphene oxide was used to encapsulate PCMs, which achieved high encapsulation rate of 85.4% [21]. Two-dimensional Mt (2D-Mt) had been used for encapsulating PCM, which contained high mass fraction (> 80%) of PCM [20]. Meanwhile, these microcapsule composite PCMs exhibited excellent thermal stability and recycle abilities. Hence, microcapsule composite PCMs based on two-dimensional materials had ultra-high heat storage capability for practical application prospect.

However, poor thermal conductivity was a key problem to restrict the practical application of microcapsule composite PCMs. Thermal conductivity of two-dimensional clay mineral encapsulated PCMs was about 0.3 W/mK [20]. Graphene oxide microcapsule phase change

* Corresponding author. School of Resources and Environmental Engineering, Wuhan University of Technology, Luoshi Road 122, Wuhan, Hubei, 430070, China.
** Corresponding author.
E-mail addresses: zyl286@whut.edu.cn (Y. Zhao), yihao287@whut.edu.cn (H. Yi).

https://doi.org/10.1016/j.solmat.2019.110090
Received 9 May 2019; Received in revised form 6 July 2019; Accepted 27 July 2019
Available online 30 July 2019
0927-0248/

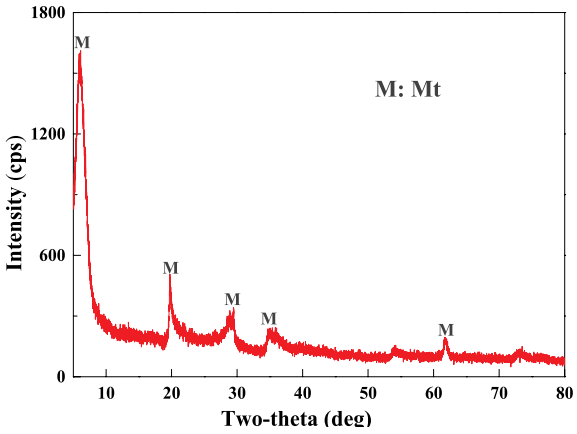

Fig. 1. XRD pattern of Mt.

material exhibited almost 0.6 W/mK in thermal conductivity [21]. Ag nanoparticles (AgNPs) decorated on graphene was used for storing PCM with only 0.4 W/mK in thermal conductivity [22]. It was noted that the thermal conductivity of composite PCMs had small promotion even by using high thermal conductive graphene shell or AgNPs loaded shell. Considering organic PCM core with very low thermal conductivity that accounted for the most volume of the composite, it was reasonable that most the microencapsulated PCMs showed very low thermal conductivity. Thus, enhancing the thermal conductivity of organic PCM in the core might be an efficient method to promote the heat transfer ability of microcapsule composite PCMs. However, few reports had studied the improvement of microcapsule composite PCMs in thermal conductivity.

Mt was considered as an excellent supporting material for shape-stabilized PCMs because of the organic compatibility, thermal reliability and outstanding porous structure [23]. Besides, montmorillonite could be exfoliated into two-dimensional nanosheets due to the swelling properties, which will contribute to the great promotion of the thermal energy storage performances [24]. Consequently, in our study, 2D-Mt was designed to encapsulate SA for increasing the mass ratio of organic PCM to promote the latent heat capacity. AgNPs were added in 2D-Mt (shell) and SA (core) to search more effective way to enhance thermal conductivity of microencapsulated phase change materials. 2D-Mt/SA microcapsule composite PCM including AgNPs was prepared for simultaneously solving low content and low thermal conductivity of organic PCM. The prepared 2D-Mt/SA/AgNPs microcapsule composite PCMs with outstanding thermal conductivity, excellent storage capacity and light-thermal conversion ability could be a prospective candidate for application in the fields of solar thermal applications.

2. Experimental

2.1. Materials

The raw Mt sample used in the work was obtained from Chifeng Ningcheng Montmorillonite Co., Ltd. In Fig. 1, high purity of Mt was proved by the X-ray diffraction spectrum (XRD). Silver nitrate, sodium dodecyl sulfate (SDS), urea, ascorbic acid, SA and hexadecyl trimethyl ammonium bromide (CTAB) used in the experiment were all of analytical grade from the Sinopharm Chemical Reagent Co., Ltd. SDS was used to enable SA latex particles negative surface charge, while CTAB was used for inducing positive surface charge on 2D-Mt surface. Ultrapure water with electrical resistivity of 18.2 MΩ cm was obtained from Millipore Super Q system.

2.2. Preparation of 2D-Mt

Mt was exfoliated into 2D-Mt as described in previous studies [25–27]. The height of 2D-Mt from substrate was around 1–2 nm measured by atomic force microscope (AFM) as showed in Fig. 2a. The inset figure displayed the height of corresponding cross-section profile of 2D-Mt marked with the line, which was acquired by the NanoScope Analysis 1.8 software. The result of thickness distribution given in Fig. 2b was obtained through randomly captured 250 images of 2D-Mt. 96.1% of 2D-Mt was less than 10 nm in thickness, indicating the successful preparation of 2D-Mt.

2.3. Preparation of Ag@2D-Mt, Ag@SA and the composite PCMs

AgNPs-decorated 2D-Mt was prepared through chemical reduction of silver nitrate by a simple hydrothermal process. Sliver nitrate solution was dropwise added in 2D-Mt suspension (3.3% 2D-Mt concentration) with constant stirring. Urea and ascorbic acid were added

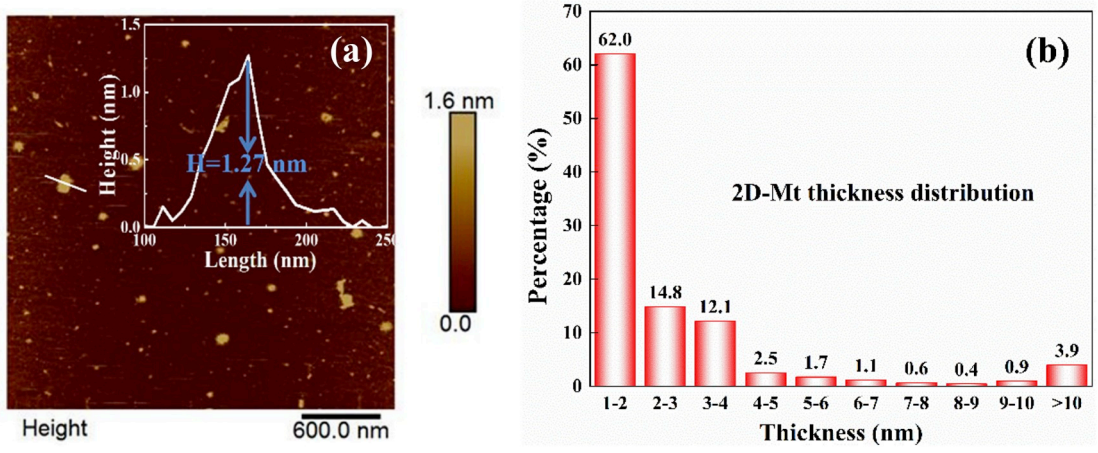

Fig. 2. Representative AFM image of 2D-Mt and the inset figure was the height of the corresponding cross-section profile marked with the line (a); thickness distribution of 2D-Mt (b).

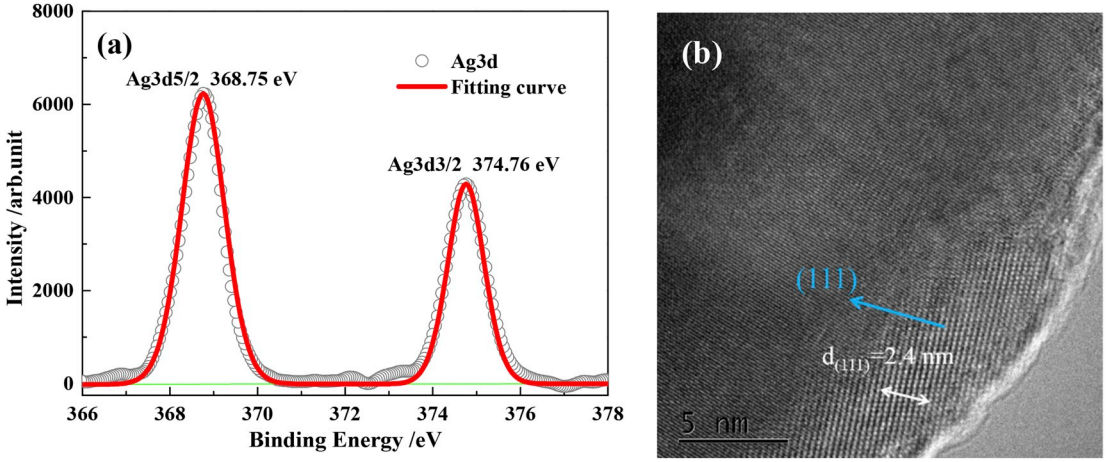

Fig. 3. High resolution XPS spectra of Ag 3d (a) and high resolution TEM of AgNPs (b) in the composite PCMs.

into the above gained solution. The mixture was heated in Teflon-lined autoclave at the temperature of 120 °C for 12 h. After cooling, washing and drying process, Ag@2D-Mt product was got. AgNPs solution was obtained by the same procedure without addition of 2D-Mt. Then Ag@SA was acquired through mixing SA with AgNPs solution for 1 h at 90 °C. The detailed fabrication of 2D-Mt/SA was exhibited in our previous study [20]. For comparison, Ag@2D-Mt/SA composite was prepared by the same procedure with replacing 2D-Mt by Ag@2D-Mt. Similarly, SA was substituted by Ag@SA to yield 2D-Mt/Ag@SA composite.

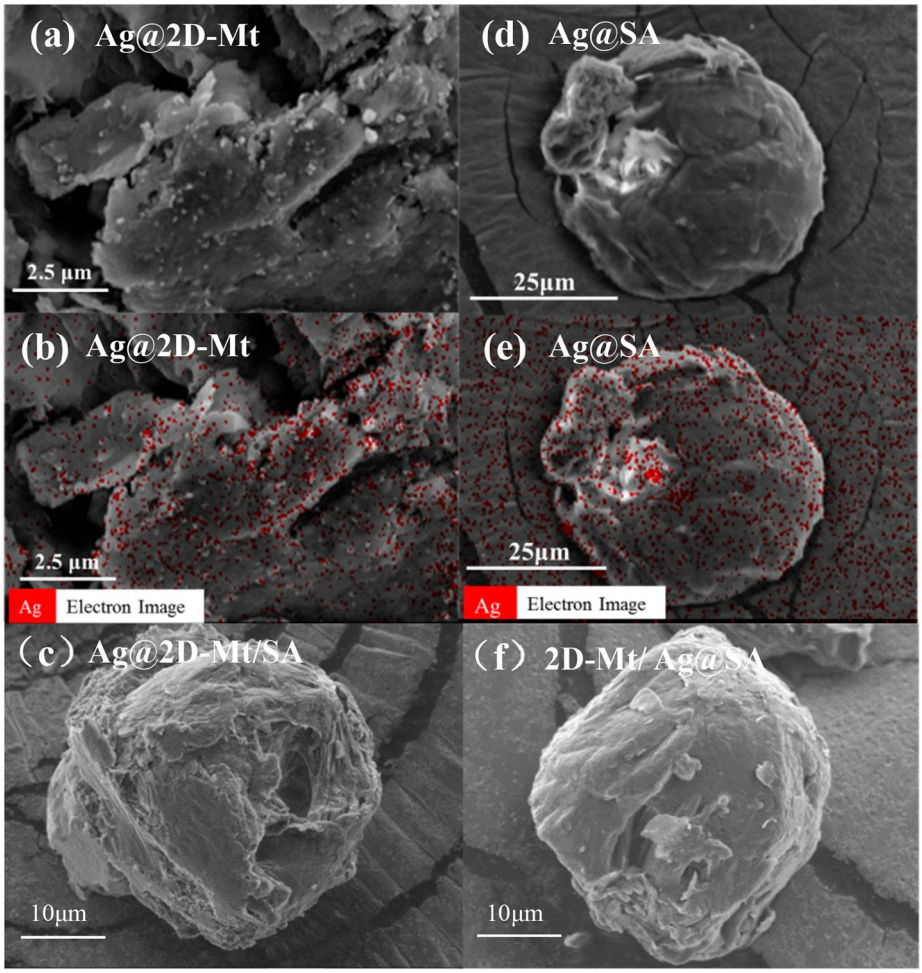

Fig. 4. SEM images of Ag@2D-Mt (a), Ag@SA (d), Ag@2D-Mt/SA (c) and 2D-Mt/Ag@SA (f); EDS elemental mapping of Ag@2D-Mt (b) and Ag@SA (e).

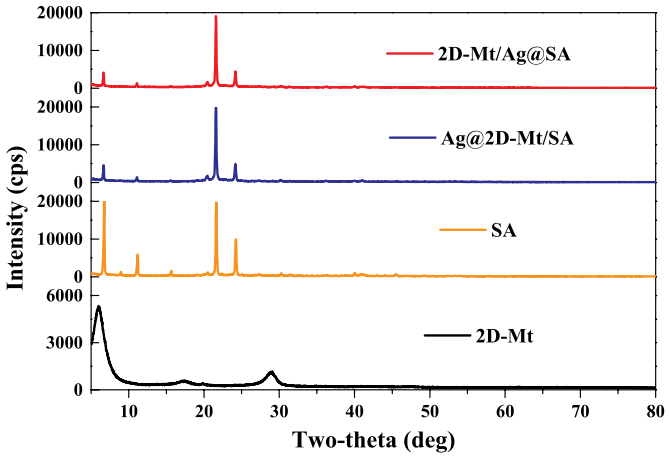

Fig. 5. XRD patterns of 2D-Mt, SA and the prepared composite PCMs.

2.4. Characterization

A D8 Advance X-ray diffractometer (Bruker AXS, Germany) was performed on recording XRD pattern of Mt, 2D-Mt, SA and composite PCMs. A Multimode 8 atomic force microscope (AFM) (Bruker, Germany) was carried out for determining thickness distribution of 2D-Mt with the peak-force tapping mode. FTIR (Thermo Nicolet, US) was used to investigate the interaction among 2D-Mt, SA and AgNPs from 4000 cm^{-1} to 400 cm^{-1}. A Zetasizer Nano (Malven, UK) was utilized for determining zeta potential of SA latex particles, SA/Ag coated by SDS, 2D-Mt, 2D-Mt/Ag and 2D-Mt/Ag modified by CTAB.

Morphologies of 2D-Mt, SA latex particles and synthesized microcapsule composite PCMs were obtained by a Zeiss Ultra Plus field-emission scanning electron microscopy (Zeiss, Germany). Meanwhile, energy-dispersive spectra (EDS) of 2D-Mt/Ag, SA/Ag and synthesized microcapsules were acquired. Image of AgNPs was characterized by JEM-2100F high-resolution transmission electron microscope.

The synthesized composite PCMs were carried out at a heating or cooling rate of 1°/min ranged from 40° to 70° by differential scanning calorimeter 8500 (PE, US). Thermogravimetric analysis (TGA) was carried out on a TA SDT Q600 thermal gravimetric analyzer under a nitrogen atmosphere. Thermal conductivity of microencapsulated PCMs was measured by TPS2500S thermal constant analyzer (Hot Disk, Sweden).

As for Light-thermal conversion tests, the visible light source was provided by a 300 W solar simulator (PLS-SXE300, Perfectlight Company, China). The cylindrical samples (~3 mm in thick and ~20 mm in diameter) were prepared by compression molding under 15 MPa. An infrared thermal imager (Fotric 224S, China) was used for directly recording the temperature distribution in the heat transfer process.

3. Results and discussion

3.1. Synthesis of 2D-Mt/SA/AgNPs microencapsulate phase change materials

XPS and high resolution TEM were applied to explore the existing status of Ag. As exhibited in Fig. 3a, two characteristic peaks of at 368.75 and 374.76 eV were belong to Ag $3d_{5/2}$ and Ag $3d_{3/2}$ orbitals, indicating that AgNPs existed in the form of metallic Ag [15]. In Fig. 3b, the lattice fringe of the AgNPs was determined to be 0.24 nm, which was corresponded to the (111) plane of fcc structure silver [28], further demonstrating the successful preparation of AgNPs. Microstructures of Ag@2D-Mt and Ag@SA were respectively showed in Fig. 4a and Fig. 4d and AgNPs were observed on 2D-Mt and SA. Corresponding EDS elemental mappings of Ag were displayed in Fig. 4b and e, demonstrating the even distribution of AgNPs on the surface of 2D-Mt and SA, respectively. Morphologies of Ag@2D-Mt/SA (Fig. 4c) and 2D-Mt/Ag@SA (Fig. 4f) indicated the microcapsule structure of composites.

XRD was applied for determining the chemical compatibility among 2D-Mt, SA and AgNPs. Fig. 5 showed the XRD patterns of 2D-Mt, SA and the prepared composite PCMs. Sharp and intense diffraction peaks at 5.996°, 17.375° and 28.929° were observed in the XRD curves of 2D-Mt. With regard to the XRD pattern of SA, the peaks at 6.668°, 11.153°, 15.619°, 21.613° and 24.022° were assigned to SA crystals. As for XRD patterns of Ag@2D-Mt/SA and 2D-Mt/Ag@SA composites, the characteristic peaks of 2D-Mt and AgNPs were not observed in the composites owing to their quite small proportion. Nevertheless, the intensity of peaks at about 6.668° of composite PCMs decreased compare with SA may due to the influence of diffraction peak at 5.996° of 2D-Mt. It was clearly that the composites exhibit same diffraction peaks with SA, which demonstrated that the composites maintained the original crystal type of SA. Sharp diffraction peaks in the composites indicated that SA in the microcapsules had high crystallinity.

To further illustrate the detailed interaction mechanisms among 2D-Mt, SA and AgNPs, FTIR and zeta potential were measured. As exhibited in Fig. 6a, typical vibrations at 464 cm^{-1} and 1032 cm^{-1} were

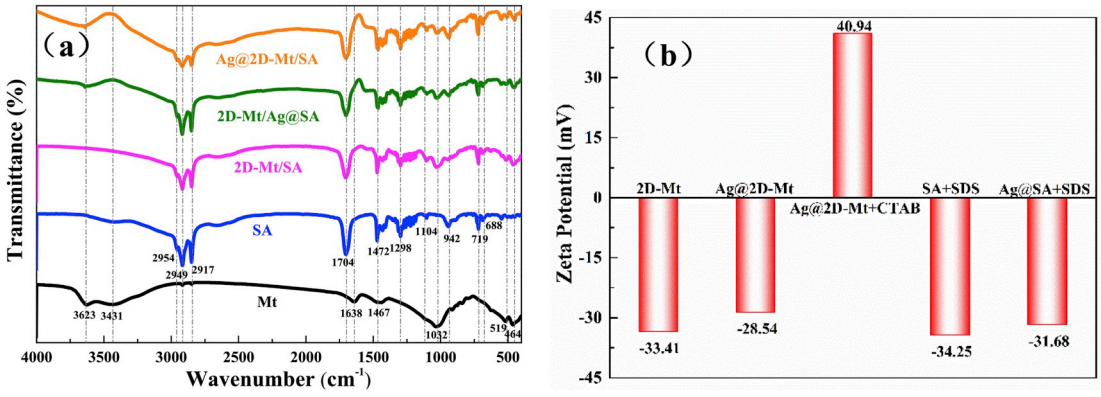

Fig. 6. FTIR spectra of Mt, SA, and the prepared composite PCMs (a), zeta potential of 2D-Mt, Ag@2D-Mt before and after adsorption of CTAB, SA stabilized by SDS, Ag@SA stabilized by SDS (b).

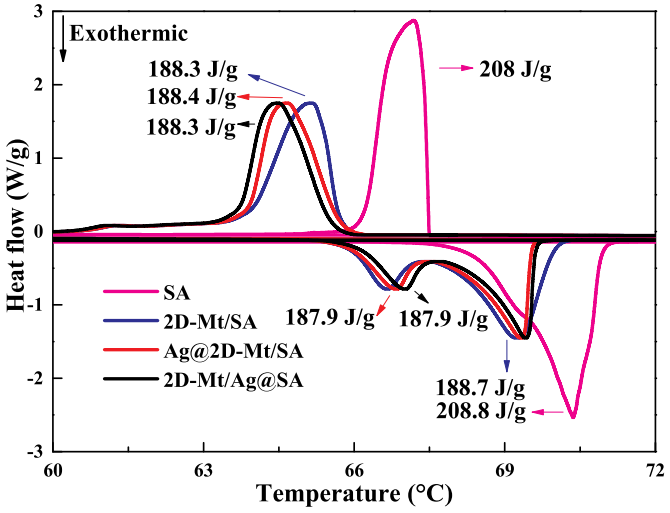

Fig. 7. DSC curves of SA and the prepared composite PCMs.

corresponded to Si-*O*-Si bending and stretching vibration of Mt, respectively [29]. With regard to SA, the characteristic peak at 1704 cm^{-1} was from carboxylic vibration (C=O) [30]. In the spectrum of composite PCMs, all the main absorption peaks of Mt and SA appeared, proving the successful combination of 2D-Mt and SA. In Fig. 6b, after modification with AgNPs, negative zeta potential of 2D-Mt (−28.54 eV) was higher than before (−33.41 eV) which might be ascribed to interaction between AgNPs and 2D-Mt. Negative charge of Ag@SA latex particles (−31.68 eV) was greater than SA particles (−34.35 eV) because of the adsorption of AgNPs in SA [31]. Meanwhile, 2D-Mt and Ag@2D-Mt rendered high positive charge after modification by CTAB. Thus, the composite PCMs were self-assembly to form core-shell structure through strong electrostatic interactions.

3.2. Latent heat capacity of 2D-Mt/SA/AgNPs

Latent heat capacity of the composite PCMs was evaluated by characterization of DSC. DSC curves of pure SA, 2D-Mt/SA, Ag@2D-Mt/SA and 2D-Mt/Ag@SA composite PCMs were outlined in Fig. 7. The melting latent heat of SA, 2D-Mt/SA, Ag@2D-Mt/SA and 2D-Mt/Ag@SA was 208 J/g, 188.3 J/g, 188.4 J/g and 188.3 J/g and related freezing latent heat of 208.8 J/g, 188.7 J/g, 187.9 J/g and 187.9 J/g, respectively. It could be noticed that the latent heat of 2D-Mt/SA, Ag@2D-Mt/SA and 2D-Mt/Ag@SA were nearly the same, demonstrating that AgNPs occupied small mass fraction in composite PCMs. The slight shift of phase change temperature was originated from interaction forces between SA core and 2D-Mt shell [16,20].As calculated, the mass ratio of SA (η) in 2D-Mt/SA, Ag@2D-Mt/SA and 2D-Mt/Ag@SA were severally 90.45%, 90.28% and 90.26%. Compared with other shape stabilized composite PCMs in Table 1, 2D-Mt/SA/AgNPs exhibited huge thermal energy storage ability that it was superior enough for practical application in solar energy storage.

3.3. Thermal conductivity of 2D-Mt/SA/AgNPs

Thermal conductivity was measured to assess the ability of heat transfer rate of composite PCMs. Thermal conductivities of SA, 2D-Mt/SA, Ag@2D-Mt/SA and 2D-Mt/Ag@SA were given in Fig. 8. As seen, thermal conductivity of 2D-Mt/SA had been greatly improved after incorporation of AgNPs. Thermal conductivity of Ag@2D-Mt/SA increased by 74.36% in terms of 2D-Mt/SA, while the thermal conductivity of 2D-Mt/Ag@SA increased by 187.82% of 2D-Mt/SA. 2D-Mt/SA@SA performed 229.3% increase in thermal conductivity compared with pure SA. It was the PCM core that limited the thermal transfer ability of microcapsule PCMs due to the large content. Thus it was reasonable that the composite PCMs with AgNPs loaded into core showed much larger thermal conductivity (increased 65.35%) than composite PCMs with AgNPs loaded into shell. The schematic illustration of thermal conduction of the prepared PCMs was shown in Fig. 9. Compared to other shape stabilized composite PCMs with SA or Mt, as displayed in Table 1, 2D-Mt/Ag@SA composite PCM revealed remarkable performance in both latent heat storage and thermal conductivity. Therefore, 2D-Mt/Ag@SA composite PCM revealed great promise for solar energy storage, building energy cycle and other sustainable energy field.

3.4. Light-thermal conversion performances of 2D-Mt/SA/AgNPs

In order to observe light-thermal performance of 2D-Mt/SA/AgNPs, the transient temperature change under sunlight radiation at 22.3 kW m^{-2} was recorded by infrared thermal camera. As illustrated in Fig. 10a, 2D-Mt/SA/AgNPs exhibited a drastically different color with pure SA and 2D-Mt/SA as time increased, which indicated a very high heating rate. During 40 s solar radiation, temperature of 2D-Mt/Ag@SA approached to phase change point, and then SA would transfer solar energy to thermal energy by phase change. 2D-Mt/Ag@SA showed a great light-thermal ability, reaching to 74 °C in 80 s while the temperature of pure SA and 2D-Mt/SA still increased without phase change. During cooling process (Fig. 10b), temperature of 2D-Mt/Ag@SA became lower than other samples over time. Also, 2D-Mt/SA/AgNPs displayed higher cooling rate than 2D-Mt/SA and pure SA. These results proved that 2D-Mt/SA/AgNPs performed very well in light-thermal conversation. Thus, 2D-Mt/SA/AgNPs had great potential in solar energy storage as an effective phase change material.

Table 1
Comparison of shape-stabilized composite PCMs in the literature.

Composite PCMs	Content of PCM (%)	Latent heat of melt (J/g)		Latent heat of freezing (J/g)	Thermal conductivity (W/mK)	Ref.
SA/Kaolin	39	66.30		53.28	–	[32]
OMt/paraffin/grafted MWNT	34.19	47.7	–		0.301	[18]
SA/doped-PANI	50.70	71.86	72.29		0.3855	[33]
SA/Mt	54.28	110	118		–	[16]
SA/W	34.7	58	64		–	[34]
SA/SiO_2	70	135.3	133.5		0.56	[11]
SA/rGO/MOF	72.62	142.4	138.1		0.6	[35]
Ag-GNS/PEG	89.67	166.1	167.8		0.414	[22]
2D-Mt/SA	82.11	184.88	181.04		0.2923	[20]
2D-Mt/Ag@SA	90.26	188.3	187.9		0.8223	This work

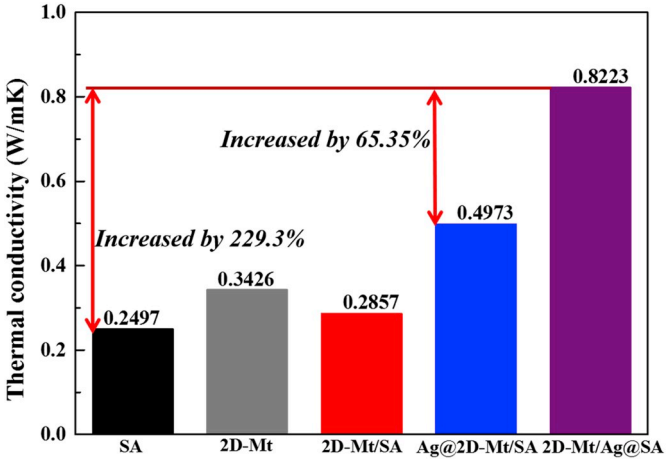

Fig. 8. Thermal conductivity of 2D-Mt, SA and the prepared composite PCMs.

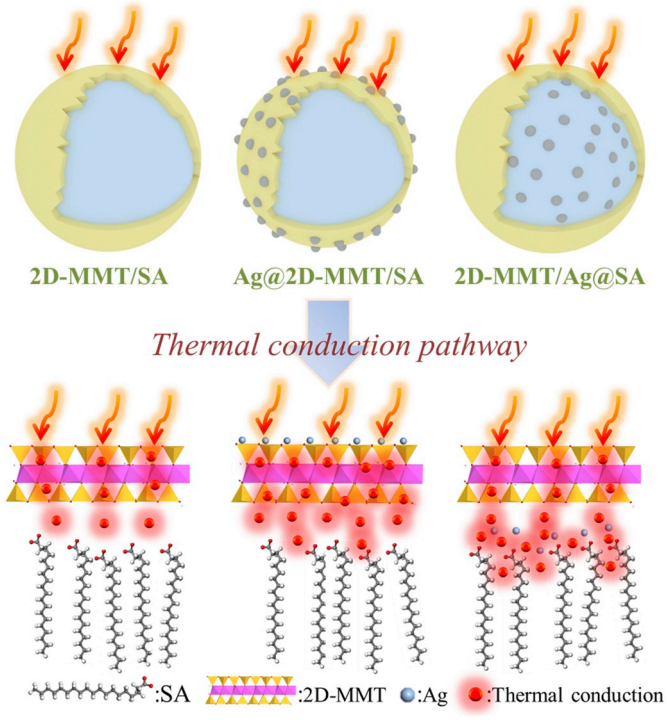

Fig. 9. Schematic illustration of thermal conduction of the prepared PCMs.

3.5. Thermal charging/discharging rate of 2D-Mt/SA/AgNPs

Boosting thermal charging/discharging rate of organic PCMs was a crux issue in unitized application of solar energy. Thermal charging/discharging rate of 2D-Mt/SA/AgNPs composites was conducted by the method of constant temperature water bath and the results were given in Fig. 11. As indicated, temperature of 2D-Mt/SA/AgNPs composites exploded upon heating and the increasing rate of temperature was apparently higher than other samples. Further, 2D-Mt/Ag@SA appeared the reduced slope at around 100 s, exhibiting appearance of phase change transition of SA. After storage process of 2D-Mt/Ag@SA, temperature of SA and 2D-Mt/SA increased yet. In cooling process, temperature of 2D-Mt/Ag@SA dropped fast and then displayed apparent stored thermal energy release procedure. Meanwhile, AgNPs doping in core performed better heat transfer than that doping in shell. Therefore, 2D-Mt/SA/AgNPs possessed remarkable charging/discharging rate.

3.6. Stability of 2D-Mt/SA/AgNPs

Tests on structural and thermal stability were carried out in this section. Fig. 12 displayed photographs of SA and the composite PCMs on a hot plate at 90 °C as time increased. It was clear that SA melt to liquid state quickly, while 2D-Mt/SA/AgNPs composites were not affected. TGA curves of SA and the composite PCMs were exhibited in Fig. 13. Thermal decomposition of SA began at around 210 °C, and all SA decomposed at about 320 °C. As for 2D-Mt/SA/AgNPs, they showed excellent thermal stability owing to no decomposition under 210 °C and the sharp loss at 210 °C could be attributed to the breaking of SA. Moreover, the residue of 2D-Mt/SA/AgNPs was approximately 7%, which was slightly lower than value measured from DSC because of dehydration process of 2D-Mt [20]. But a conclusion could still be drawn that the weight fraction of SA in the composite PCMs accorded well with the results obtained according to DSC. Thus, AgNPs hardly affect the structural and thermal stability of composite PCMs. Core-shell structure of 2D-Mt/SA/AgNPs was excellent for the restriction of leakage.

3.7. Cycling performances of 2D-Mt/SA/AgNPs

The prepared composite PCMs should possess thermal stability over quantities of heating/cooling cycles. Hence, 100 times heating/cooling cycling tests were performed on determining the change in structure and thermal properties of 2D-Mt/SA/AgNPs composites. Fig. 14a-b showed SEM images of 2D-Mt/SA/AgNPs after heat/cooling cycling experiments. The composite PCMs still retained the microcapsule structure, which suggested no degradation of composite PCMs occurred during heating/cooling cycling process. DSC curves of 2D-Mt/SA/

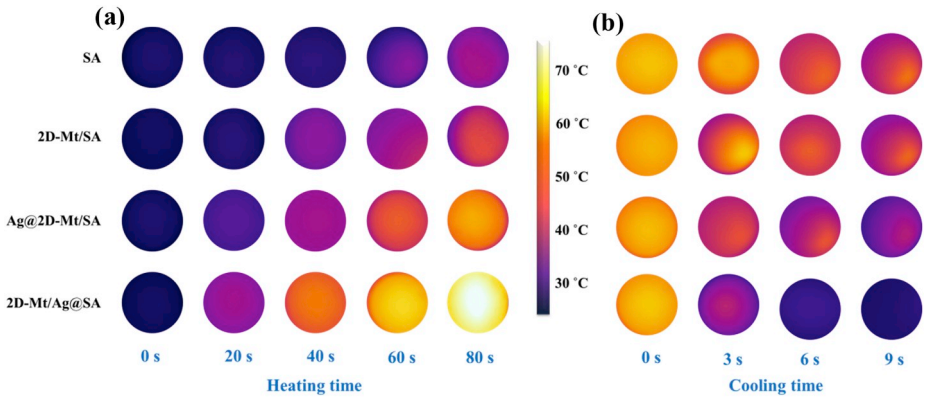

Fig. 10. Temperature response of pure SA and composite PCMs at different heating times (a) and cooling times (b).

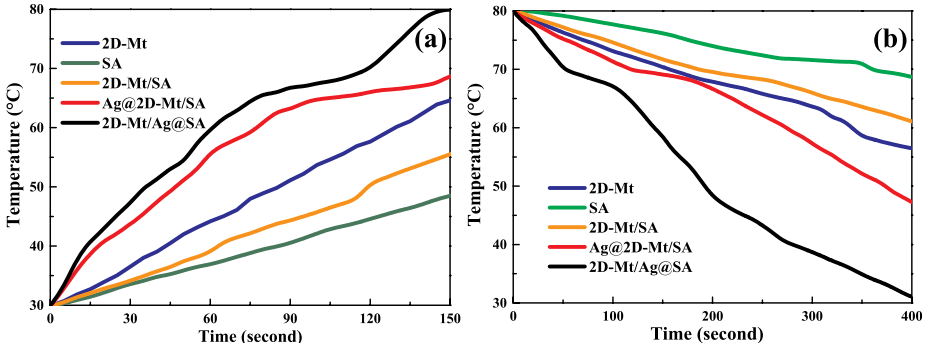

Fig. 11. Thermal charging/discharging rate of SA, 2D-Mt and composite PCMs.

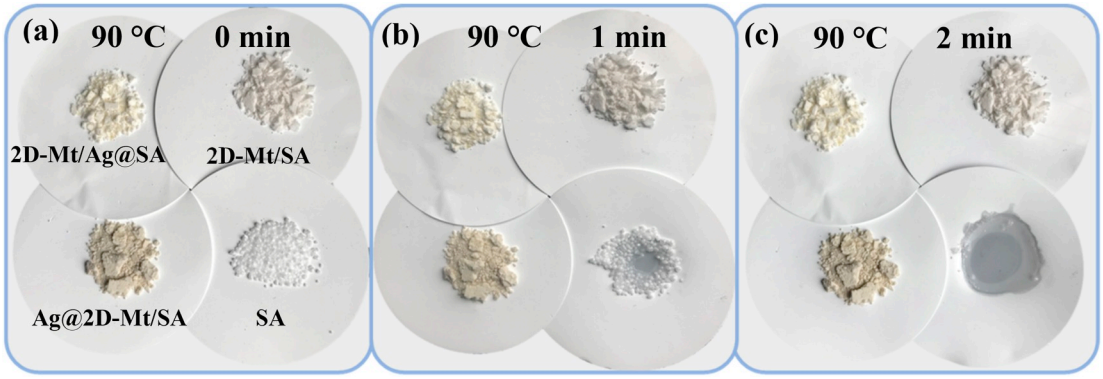

Fig. 12. The photographs of SA and the prepared composite PCMs on a hot plate at 90 °C.

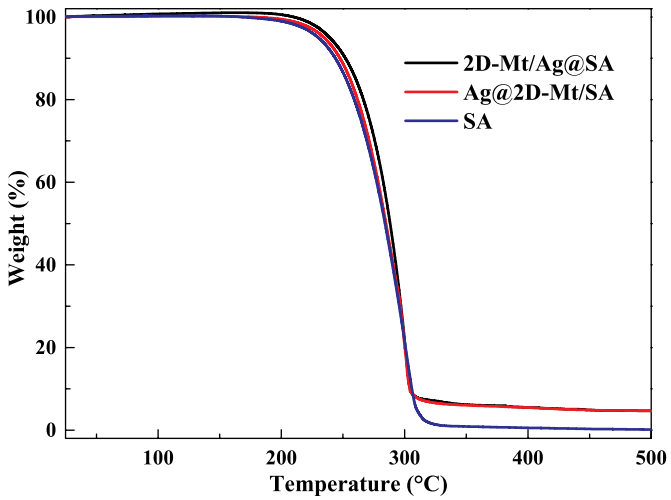

Fig. 13. TGA curves of SA and 2D-Mt/SA/AgNPs composites.

AgNPs before and after repeating heating/cooling cycles were given in Fig. 14c-d. Obviously, little changes occurred in the latent heat of the composite PCMs. Fig. 14e exhibited the comparison consequences of thermal conductivity of the composite PCMs before and after thermal cycles. There were almost no variations in the aspect of heat transfer. In summary, 2D-Mt/SA/AgNPs composite PCMs had excellent heating/cooling cycling performance, which could be used as an excellent heat energy storage material in sustainable energy field.

4. Conclusions

(1) 2D-Mt/SA/AgNPs showed dramatic latent heat storage of 187 J/g due to more than 90 wt% loading of SA.
(2) Thermal conductivity of 2D-Mt/SA/AgNPs (0.8223 W/mK) has increased 229.3% when AgNPs was incorporated into the PCM core.
(3) 2D-Mt/SA/AgNPs displayed excellent thermal charging/discharging rate and outstanding photo-thermal conversion efficiency.
(4) 2D-Mt/SA/AgNPs were proved to show good thermal stability and superior cycling performances.

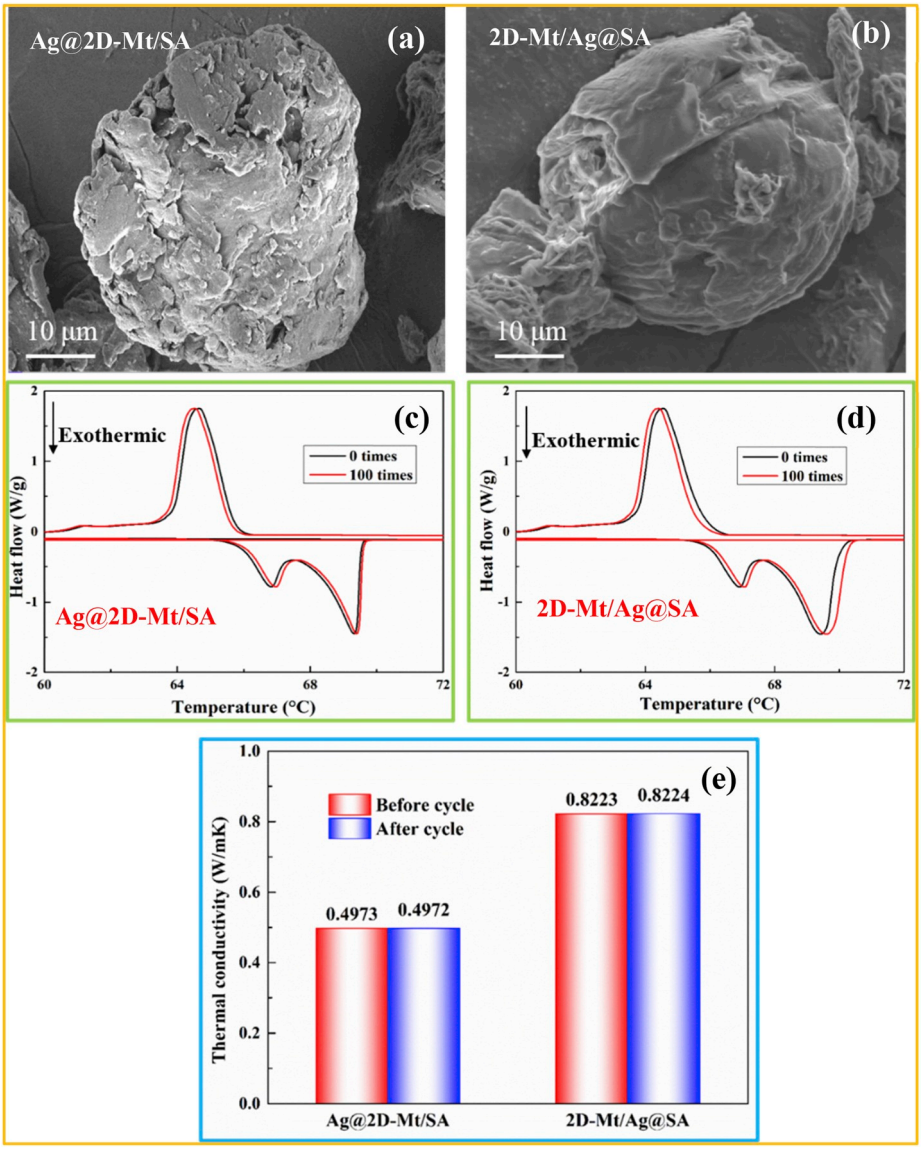

Fig. 14. Characterization of 2D-Mt/SA/AgNPs composites after 100 times heating/cooling cycles, SEM images (a–b), DSC curves (c–d) and thermal conductivity (e).

Acknowledgements

The financial supports to this work from the National Natural Science Foundation of China (projects No. 51674183 and 51874220) and the Natural Science Foundation of Hubei Province of China (2018CFB468) are gratefully acknowledged. Y. Zhao also thanks the China Scholarship Council for the academic staying in USA (File No. 201806955006).

Appendix A. Supplementary data

Supplementary data to this article can be found online at https://doi.org/10.1016/j.solmat.2019.110090.

References

[1] D.Q. Ng, Y.L. Tseng, Y.F. Shih, H.Y. Lian, Y.H. Yu, Synthesis of novel phase change material microcapsule and its application, Polymer 133 (2017) 250–262, https://doi.org/10.1016/j.polymer.2017.11.046.

[2] S. Baddadi, S. Bouadila, W. Ghorbel, A.A. Guizani, Autonomous greenhouse microclimate through hydroponic design and refurbished thermal energy by phase change material, J. Clean. Prod. 211 (2019) 360–379, https://doi.org/10.1016/j.jclepro.2018.11.192.

[3] J. Yang, L. Tang, R. Bao, L. Bai, Z. Liu, B. Xie, M. Yang, Hybrid network structure of boron nitride and graphene oxide in shape- stabilized composite phase change materials with enhanced thermal conductivity and light-to-electric energy conversion capability, Sol. Energy Mater. Sol. Cells 174 (2018) 56–64 https://doi.org/10.1016/j.solmat.2017.08.025.

[4] Y. Chen, Q. Zhang, X. Wen, H. Yin, J. Liu, A novel CNT encapsulated phase change material with enhanced thermal conductivity and photo-thermal conversion performance, Sol. Energy Mater. Sol. Cells 184 (2018) 82–90, https://doi.org/10.1016/j.solmat.2018.04.034.

[5] J.D. Xiao, H.L. Jiang, Metal-organic frameworks for photocatalysis and photothermal catalysis, Acc. Chem. Res. 52 (2018) 356–366, https://doi.org/10.1021/acs.accounts.8b00521.

[6] X. Zhang, C. Liu, Z. Rao, Experimental Investigation on Thermal Management Performance of Electric Vehicle Power Battery Using Composite Phase Change Material, Elsevier Ltd, 2018, https://doi.org/10.1016/j.jclepro.2018.08.076.

[7] A.K. Pandey, M.S. Hossain, V. V Tyagi, N. Abd, J.A.L. Selvaraj, A. Sari, Novel approaches and recent developments on potential applications of phase change materials in solar energy, Renew. Sustain. Energy Rev. 82 (2018) 281–323 https://doi.org/10.1016/j.rser.2017.09.043.

[8] S. Song, F. Qiu, W. Zhu, Y. Guo, Y. Zhang, Y. Ju, R. Feng, Y. Liu, Z. Chen, J. Zhou, C. Xiong, L. Dong, Polyethylene glycol/halloysite@Ag nanocomposite PCM for thermal energy storage: simultaneously high latent heat and enhanced thermal conductivity, Sol. Energy Mater. Sol. Cells 193 (2019) 237–245, https://doi.org/10.1016/j.solmat.2019.01.023.

[9] M. Emam, M. Ahmed, Cooling concentrator photovoltaic systems using various configurations of phase-change material heat sinks, Energy Convers. Manag. 158 (2018) 298–314 https://doi.org/10.1016/j.enconman.2017.12.077.

[10] S. Manikandan, C. Selvam, N. Poddar, K. Pranjyal, R. Lamba, S.C. Kaushik, Thermal

management of low concentrated photovoltaic module with phase change material, J. Clean. Prod. 219 (2019) 359–367, https://doi.org/10.1016/j.jclepro.2019.02.086.
[11] S. Fan, H. Gao, W. Dong, J. Tang, J. Wang, M. Yang, G. Wang, Shape-stabilized phase change materials based on stearic acid and mesoporous hollow SiO_2 microspheres (SA/SiO_2) for thermal energy storage, Eur. J. Inorg. Chem. 2017 (2017) 2138–2143.
[12] C. Lamnatou, F. Motte, G. Notton, D. Chemisana, C. Cristofari, Building-integrated solar thermal system with/without phase change material: life cycle assessment based on ReCiPe, USEtox and Ecological footprint, J. Clean. Prod. 193 (2018) 672–683, https://doi.org/10.1016/j.jclepro.2018.05.032.
[13] X. Zhang, Z. Yin, D. Meng, Z. Huang, R. Wen, Y. Huang, X. Min, Y. Liu, M. Fang, X. Wu, Shape-stabilized composite phase change materials with high thermal conductivity based on stearic acid and modified expanded vermiculite, Renew. Energy 112 (2017) 113–123, https://doi.org/10.1016/j.renene.2017.05.026.
[14] J. Chen, J. Li, H. Wang, W. Huang, W. Sun, T. Xu, Preparation and effectiveness of composite phase change material for performance improvement of Open Graded Friction Course, J. Clean. Prod. 214 (2019) 259–269, https://doi.org/10.1016/j.jclepro.2019.01.001.
[15] T. Qian, J. Li, X. Min, W. Guan, Y. Deng, L. Ning, Enhanced thermal conductivity of PEG/diatomite shape-stabilized phase change materials with Ag nanoparticles for thermal energy storage, J. Mater. Chem. A. 3 (2015) 8526–8536.
[16] K. Peng, L. Fu, X. Li, J. Ouyang, H. Yang, Stearic acid modified montmorillonite as emerging microcapsules for thermal energy storage, Appl. Clay Sci. 138 (2017) 100–106 https://doi.org/10.1016/j.clay.2017.01.003.
[17] B. Xu, H. Ma, Z. Lu, Z. Li, Paraffin/expanded vermiculite composite phase change material as aggregate for developing lightweight thermal energy storage cement-based composites, Appl. Energy 160 (2015) 358–367 https://doi.org/10.1016/j.apenergy.2015.09.069.
[18] M. Li, Q. Guo, S. Nutt, Carbon nanotube/paraffin/montmorillonite composite phase change material for thermal energy storage, Sol. Energy 146 (2017) 1–7 https://doi.org/10.1016/j.solener.2017.02.003.
[19] B. Mu, M. Li, Synthesis of novel form-stable composite phase change materials with modified graphene aerogel for solar energy conversion and storage, Sol. Energy Mater. Sol. Cells 191 (2019) 466–475, https://doi.org/10.1016/j.solmat.2018.11.025.
[20] H. Yi, W. Zhan, Y. Zhao, S. Qu, W. Wang, P. Chen, S. Song, A novel core-shell structural montmorillonite nanosheets/stearic acid composite PCM for great promotion of thermal energy storage properties, Sol. Energy Mater. Sol. Cells 192 (2019) 57–64 https://linkinghub.elsevier.com/retrieve/pii/S0927024818305816.
[21] K. Yuan, J. Liu, X. Fang, Z. Zhang, Novel facile self-assembly approach to construct graphene oxide-decorated phase-change microcapsules with enhanced photo-to-thermal conversion performance, J. Mater. Chem. A. 6 (2018) 4535–4543, https://doi.org/10.1039/c8ta00215k.
[22] Y. Zhang, J. Wang, J. Qiu, X. Jin, M.M. Umair, R. Lu, S. Zhang, B. Tang, Ag-graphene/PEG composite phase change materials for enhancing solar-thermal energy conversion and storage capacity, Appl. Energy 237 (2019) 83–90, https://doi.org/10.1016/j.apenergy.2018.12.075.
[23] H. Yi, F. Jia, Y. Zhao, W. Wang, S. Song, H. Li, C. Liu, Surface wettability of montmorillonite (0 0 1) surface as affected by surface charge and exchangeable cations: a molecular dynamic study, Appl. Surf. Sci. 459 (2018) 148–154, https://doi.org/10.1016/j.apsusc.2018.07.216.
[24] H. Yi, W. Zhan, Y. Zhao, X. Zhang, F. Jia, W. Wang, Z. Ai, S. Song, Design of MtNS/SA microencapsulated phase change materials for enhancement of thermal energy storage performances: effect of shell thickness, Sol. Energy Mater. Sol. Cells 200 (2019) 109935, , https://doi.org/10.1016/j.solmat.2019.109935.
[25] W. Wang, Y. Zhao, H. Yi, T. Chen, S. Kang, H. Li, S. Song, Preparation and characterization of self-assembly hydrogels with exfoliated montmorillonite nanosheets and chitosan, Nanotechnology 29 (2018) 1–11.
[26] Y. Zhao, H. Yi, F. Jia, H. Li, C. Peng, S. Song, A novel method for determining the thickness of hydration shells on nanosheets: a case of montmorillonite in water, Powder Technol. 306 (2017) 74–79 https://doi.org/10.1016/j.powtec.2016.10.045.
[27] W. Wang, Y. Zhao, H. Bai, T. Zhang, V. Ibarra-Galvan, S. Song, Methylene blue removal from water using the hydrogel beads of poly(vinyl alcohol)-sodium alginate-chitosan-montmorillonite, Carbohydr. Polym. 198 (2018) 518–528 https://doi.org/10.1016/j.carbpol.2018.06.124.
[28] S. Dhivya, S.I. Hussain, S. Jeya Sheela, S. Kalaiselvam, Experimental study on microcapsules of Ag doped ZnO nanomaterials enhanced Oleic-Myristic acid eutectic PCM for thermal energy storage, Thermochim. Acta 671 (2019) 70–82, https://doi.org/10.1016/j.tca.2018.11.010.
[29] S. Kang, Y. Zhao, W. Wang, T. Zhang, T. Chen, H. Yi, F. Rao, S. Song, Removal of methylene blue from water with montmorillonite nanosheets/chitosan hydrogels as adsorbent, Appl. Surf. Sci. 448 (2018) 203–211, https://doi.org/10.1016/j.apsusc.2018.04.037.
[30] T.D. Dao, H.M. Jeong, A Pickering emulsion route to a stearic acid/graphene core e shell composite phase change material, Carbon N. Y. 99 (2016) 49–57 https://doi.org/10.1016/j.carbon.2015.12.009.
[31] C. Dong, X. Zhang, H. Cai, C. Cao, K. Zhou, X. Wang, Synthesis of stearic acid-stabilized silver nanoparticles in aqueous solution, Adv. Powder Technol. 27 (2016) 1–8 https://doi.org/10.1016/j.apt.2016.08.018.
[32] S. Liu, H. Yang, Stearic acid hybridizing coal-series kaolin composite phase change material for thermal energy storage, Appl. Clay Sci. 101 (2014) 277–281 https://doi.org/10.1016/j.clay.2014.09.002.
[33] Y. Wang, H. Ji, T. Zhang, H. Shi, D. Zhang, H. Feng, Effect of fabrication methodology on morphology , conductivity , and thermal-energy storage of a stearic acid/doped-polyaniline phase-change material, Energy Technol. 730050 (2015) 734–742.
[34] D. Xu, H. Yang, Wollastonite hybridizing stearic acid as thermal energy storage material, Funct. Mater. Lett. 7 (2014) 1–4.
[35] A. Li, C. Dong, W. Dong, D.G. Atinafu, H. Gao, X. Chen, G. Wang, Hierarchical 3D reduced graphene porous-carbon-based PCMs for superior thermal energy storage performance, ACS Appl. Mater. Interfaces 10 (2018) 32093–32101.